JOURNAL OF MATERIALS SCIENCE 31 (1996) 2839–2847

Pulsed laser deposition of silicon nitride thin films by laser ablation of a Si target in low pressure ammonia

I.N. MIHAILESCU, ADRIANA LITA, V.S. TEODORESCU
Institute of Atomic Physics, Laser Department, P.O. Box MG-54, RO-76900 Bucharest, Romania

A. LUCHES, M. MARTINO, A. PERRONE
Department of Physics, University of Lecce, Italy

MARIA GARTNER
Institute of Chemical Physics, Bucharest, Romania

We report the deposition of Si–N films by multipulse excimer laser ($\lambda = 308$ nm, $\tau_{FWHM} = 30$ ns) ablation of Si wafers placed in a slow flow of NH_3 in the pressure range (1 μbar–1 mbar). The films are deposited on to a Si collector placed parallel to the Si target. We succeeded in depositing pure amorphous Si_3N_4 films at a pressure of 1 mbar of NH_3. The deposition rate reached a maximum value of 0.2–0.3 nm per pulse. At lower pressures, the deposited films consist of a fine mixture of three amorphous phases (amorphous stoichiometric silicon nitride, amorphous non-stoichiometric silicon nitride and amorphous silicon). The amorphous silicon is prevalent in films deposited at a pressure of several to several tens of μbars. Droplets of polycrystalline α-Si are sometimes visible on the film surface. The experimental evidence, is analysed with a view to elucidating the participation in the chemical synthesis of the three main stages of the process: the substance expulsion from the target by laser ablation, the transition through the gas of the expulsed substance and it's final impact on the collector. We conclude that silicon nitride is mostly synthesized during the impact on the collector of the flow of the ablated substance.

1. Introduction

Silicon nitride exhibits an advantageous combination of several challenging performance requirements [1,2]. Firstly, silicon nitride has a good chemical stability at rather high temperatures. In addition, it has a high resistance to mechanical shock and remarkable corrosion wear. Silicon nitride is a light material (having a density of 3190 kg m^{-3}). It is characterized by a quite low value of the dilatation coefficient and exhibits a very high resistivity (larger than 10^{14} Ω cm). Silicon nitride behaves therefore as an electrical insulator in very thin layers.

Due to these features, silicon nitride is intensively used in advanced technologies [3]. Si_3N_4 is employed in the preparation of special ceramics, mechanical constructions and also as a refractory material where corrosion resistance is needed and also as an electrical insulator. We also note the use of thin films of silicon nitride in VLSI microelectronics where they find use in a variety of applications; for example in multilevel interconnect structures, barrier layers and especially in the final passivation of many types of structures [4, 5].

Lasers have been applied to the synthesis of silicon nitride as either a powder or in thin film form [6]. The most commonly reported procedure concerns the laser pyrolysis of SiH_4 and NH_3 precursors [7]. Thin Si_3N_4 layers were obtained by photolysis, using either an excimer laser [8] or lamps [4, 9, 10]. In most of the cases, the reaction takes place in a homogeneous phase and evolves away from the chamber walls. The silicon nitride powder formed is spread in all directions. As a result, a part of the synthesized powder is lost and optical elements in the growth chamber can be irreversible damaged.

We have succeeded in synthesizing a silicon nitride thin layer in a heterogeneous phase reaction by laser direct synthesis [11, 12]. To this aim, silicon wafers were submitted to a long multipulse irradiation series in an NH_3 atmosphere. Thin layers of very pure a-Si_3N_4 were formed on a Si surface after the action of several thousand laser pulses. The thickness of the synthesized layer is limited to 3–5 μm due to saturation. Unfortunately, the prolonged multipulse laser irradiation causes surface perturbations which remain visible at the end of the laser treatment in the form of surface ripples. These ripples which are typically in the μm size range are undesirable for microelectronic applications.

A new technique [13–18] the Laser Reactive Ablation (LRA) overcomes these drawbacks. It consists of

0022–2461 © 1996 Chapman & Hall

the laser ablation of a target in a complex process accompanied by chemical reactions in an ambient atmosphere of a low pressure reactive gas. Reaction products are collected on an additional support. The thickness of the deposited film is unlimited and can be smoothly increased through the cumulative action of an appropriate number of laser pulses. The films are protected against the perturbing action of the plasma and/or of the shock waves and are therefore free of ripples or other roughness. The heating of either the target or the collecting support is not mandatory.

We have reported [19, 20] the application of LRA to the synthesis and deposition of silicon nitride films. We continue here with further experimental and theoretical data concerning such films.

2. Experimental procedure

The general experimental scheme is depicted in Fig. 1. The experiments were performed with the aid of a Lambda Physik LPX 315i XeCl* excimer laser ($\lambda = 308$ nm, $\tau_{FWHM} = 30$ ns). The Si wafers, were submitted to series of 10^4 laser pulses, at a repetition rate of 10 Hz. The incident laser fluence was set with the aid of a focusing lens (L) at a value $E_s > 5$ J cm^{-2}. The laser beam was incident under an angle of $\sim 45°$ to the normal of the Si target surface. The target was rotated at a frequency of 3 Hz in order to avoid fast drilling. The ablated material was collected on a $\langle 100 \rangle$ Si wafer surface placed at varying distances from the target, of $d = 14, 21$ and 30 mm. In order to improve the adherence of the deposited films, a ceramic heater (H) is embedded into the collector. The Si collector was generally heated to 200 °C. The reaction chamber was first evacuated down to a residual pressure of $\sim 10^{-7}$ mbar. Then, the chamber was filled with

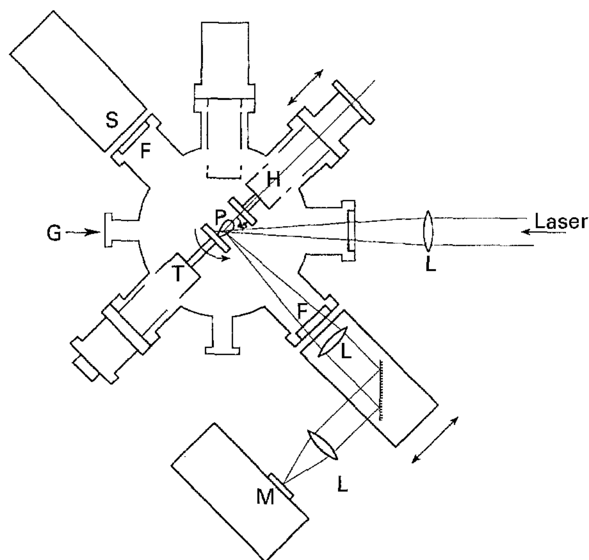

Figure 1 Schematic diagram of the experimental apparatus. (T)-Rotatable target-holder; (H) Heated substrate holder; (L) Focusing lens; (P) Plasma plume; (F) Lens; (G) Gas (NH_3) inlet; (M) Monochromator; (S) Spectrograph.

electronic grade ammonia. The NH_3 pressure was set at five different values in the range 1×10^{-3}–1 mbar: $p_0 = 1, 10, 50$ µbar and 0.1, 1 mbar, respectively.

Time-integrated optical emission spectra (OES) of the plasma (P) evolving in front of the Si target were recorded. An integral spectrum ranging from 360–600 nm was recorded during a complete multipulse irradiation series. The time–resolved evolution of characteristic lines of neutral and ionized silicon were detected. To this purpose a suprasil lens (F), was used for imaging the plasma on the 50-µm-wide entrance slit of a grating spectrograph (S), (model S100 from Oriel Optik). The deposited films were investigated with different techniques in order to have a better understanding of the phenomena involved in the LRA of Si in NH_3. The films were investigated by transmission electron microscopy (TEM) and selected area electron diffraction (SAED) with the aid of a Jeol Temscan 200 CX electron microscope. For TEM and SAED investigations, representative specimens were prepared by extraction replica methods.

Due to their potential important practical applications, the films were also optically studied by spectroscopic ellipsometry (SE) [21, 22]. In our case, SE analyses, were conducted with the Bruggeman effective media approximation (EMA) [23–25]. The SE investigations of the films were conducted with the aid of a variable angle ellipsometer in uv-vis mode. The apparatus allowed a reading accuracy of 1 minute for both azimuths (polarizer and analyser) and for the angle of incidence.

Electron spectroscopic studies were performed with a view to characterize both the films deposited by LRA on the collector and also the crater formed on the surface of the Si sample during the laser ablation. These studies were accomplished with the aid of a Escalab Mk II (V.G. Scientific) apparatus, whose analysis chamber was evacuated down to 10^{-10} mbar. The unmonochromated AlK_α radiation of 1486.6 eV was used for recording the X-ray photoelectron spectroscopy (XPS) spectra. We recorded the photoelectron spectrum corresponding to the Si 2p level in the range 90–110 eV. The spectra calibration was obtained against the Ag $3d_{5/2}$ ($E_b = 368.26$ eV) and Ag M_4NN ($E_b = 1128.78$ eV) lines with the Fermi level as the control energy. The correction for charge effects was ensured with a flood gun, as against the position of the C 1s line (285 eV). For a clear identification of the chemical bonds we also recorded the Auger transition (X-ray Auger electron spectroscopy-XAES) Si KLL at 1600–1650 eV.

3. Results

3.1. OES experiments

A first observation is that a bright spark accompanies the action of every laser pulse. A second observation is that the OES spectra contains lines which belong to three Si species – Si III, Si II and Si I (Fig. 2). From the time-resolved spectra at various distances from the target surfaces one can calculate both the velocities

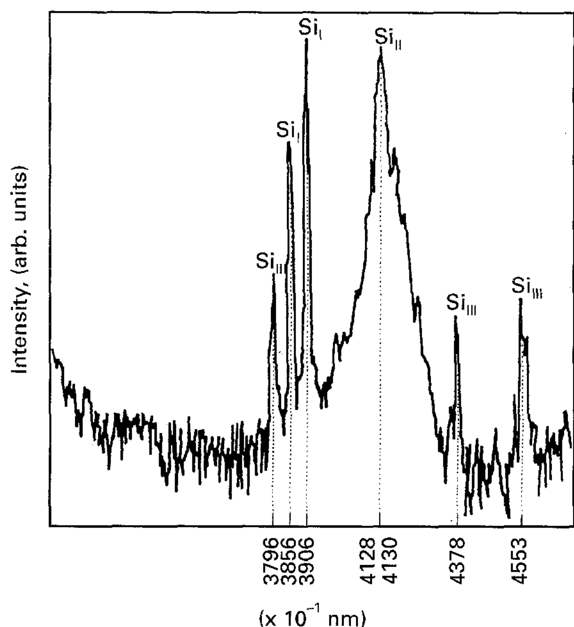

Figure 2 The Time-integrated optical emission spectrum of the plasma evolving in front of the Si target at a pressure of $p_0 = 1$ mbar of ambient NH_3.

and the kinetic energies of either neutral or ionized Si atoms in the plasma plume. We obtained mean velocities of $\sim 2.4 \times 10^4$ ms^{-1} for SiI and of $\sim 1.8 \times 10^4$ ms^{-1} for SiII. No lines corresponding to nitrogen species were observed in any of the time-integrated OES.

3.2. Visual and profilometric experiments

Visual inspection of the films deposited on the collector after the action of several tens to several hundreds of laser pulses shows they are brightly coloured from pale yellow to green or violet. When the irradiation series is prolonged to several thousands of pulses, the colour of the films stabilizes to dull grey in contrast to the brilliant grey of the neighbouring uncoated silicon zones on the collector surface. The homogeneous character of the deposition was observed by scanning the films with a profilometer needle. Typical recordings are shown in Fig. 3(a,b). From Fig. 3a, we notice that the film thickness was resonably constant. The film thickness depends strongly on the target-collector separation distance. Films of 2–3 μm were deposited for $d = 14$ mm (Fig. 3b). The thickness diminishes to 0.2–0.3 μm at $d = 30$ mm (Fig. 3a). For $d = 21$ mm, the deposited films have a thickness of 1–1.5 μm. Peaks are more abundant and larger in the case of films obtained at $d = 14$ mm (compare Fig. 3a, b).

The dependence of the deposited film thickness on the gas pressure is much weaker. The thickness of the deposited films decreases up to 50 per cent at $d = 14$ mm and $d = 21$ mm and 70 per cent at $d = 30$ mm when increasing p_0 from 1 μbar to 1 mbar. The peaks are much more numerous at small pressures of 1–10 μbar than at 1 mbar.

3.3. Electron microscopy studies

Analysis of the TEM and SAED. patterns were performed with the aid of standard samples of amorphous silicon nitride, amorphous silicon and of amorphous silicon dioxide.

A general observation concerns the rather amorphous character of the films. The films obtained at $p_0 = 1$ mbar are completely amorphous while the films deposited at smaller ambient pressures include crystalline islands. There is one amorphous compound which has been observed in all the films prepared by LRA. This compound exhibits in diffraction studies (curve a in Fig. 4) two halos with maxima corresponding to effective interplanar distances of 0.35 ± 0.01 nm and 0.14 nm, respectively – i.e. close to the positions of 0.36 ± 0.01 nm and 0.13 nm of the halos observed in case of the standard of amorphous silicon nitride (curve b in Fig. 4). The quantity of a-Si_3N_4 increases with the pressure of the gas in which the Si ablation was promoted.

Amorphous Si is present in some of the films. We observed amorphous silicon with a structure identical to that of the standard prepared by thermal evaporation in vacuum. The diffraction patterns for both of them exhibit two distinct halos with maxima corresponding to effective interplanar distances of 0.315 ± 0.005 nm and 0.175 nm, respectively. An identical pattern was observed in the case of the film deposited by laser ablation of silicon in a vacuum.

Finally, a third amorphous compound was identified in the films deposited at small and intermediate pressures. The diffraction studies of this compound

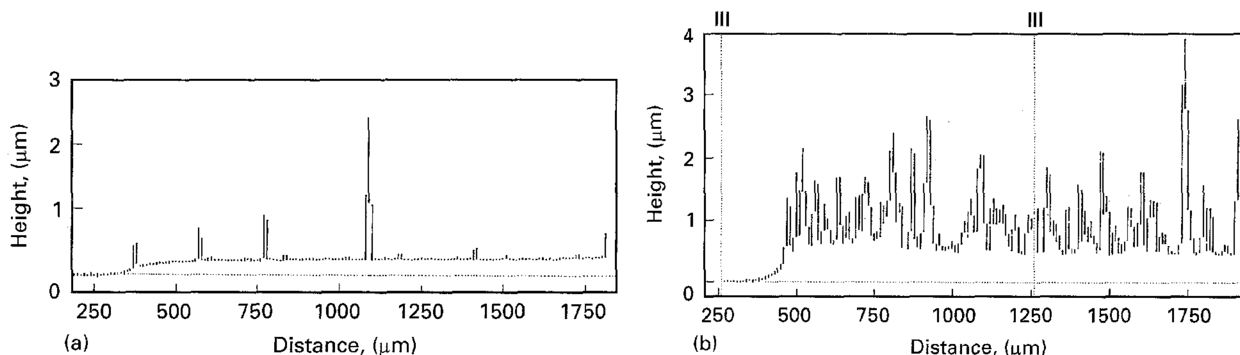

Figure 3 Profilometer recordings of films deposited at a pressure of $p_0 = 1$ μbar of ambient NH_3. The target-collector distance was $d = 30$ mm (a) and at $d = 14$ mm (b), respectively.

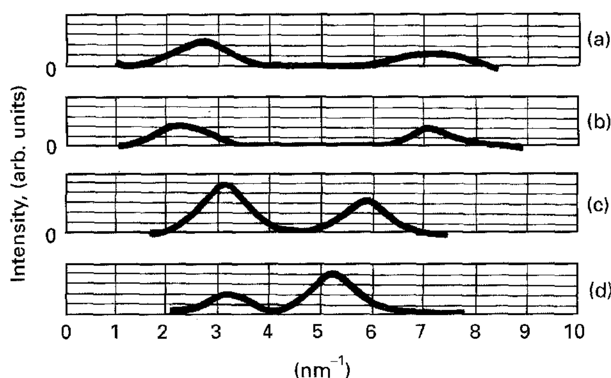

Figure 4 The intensity distribution in the electron diffraction patterns after subtraction of the incoherent continuum intensity in case of:
(a) the amorphous silicon nitride films deposited at $p_0 = 1$ mbar and $d = 30$ mm. (b) the sample of amorphous silicon nitride prepared by LCVD; (c) the amorphous silicon in a film deposited at $p_0 = 10$ µbar and $d = 14$ mm and the sample of amorphous silicon prepared by thermal evaporation in vacuum.
(d) the third amorphous compound (most probably amorphous nonstoichiometric silicon nitride, SiN_x). The pattern in the figure is recorded when examining the film obtained at $p_0 = 10$ µbar and $d = 30$ mm.

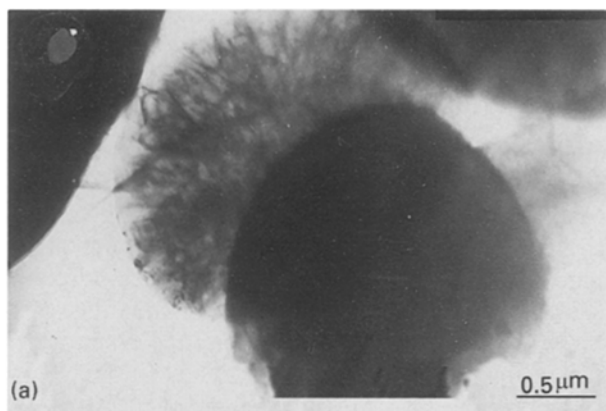

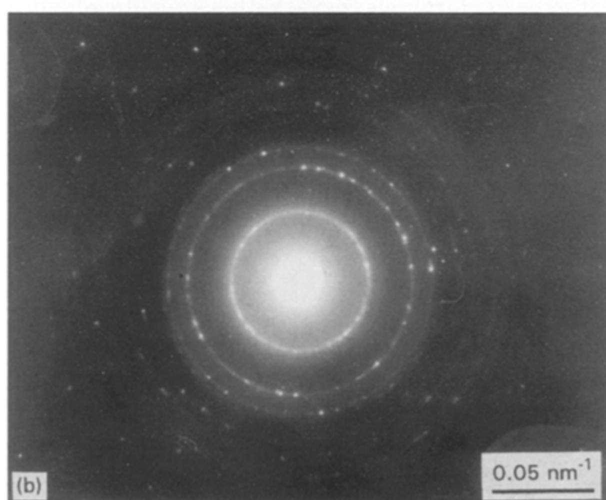

Figure 5 (a) A TEM micrograph of an area of the film deposited at $p_0 = 1$ µbar and $d = 14$ mm. Droplets of various dimensions are visible. (b) SAED pattern of the droplets visible in Fig. 5a.

exhibit two halos with maxima corresponding to effective interplanar distances of 0.320 ± 0.005 nm and 0.205 nm, respectively (curve d in Fig. 4). We note that this amorphous compound has a structure completely different to that of amorphous Si or that of amorphous silicon dioxide. We conclude that this compound which is similar to a certain extent with amorphous silicon nitride, is in fact a nonstoichiometric silicon nitride of the type SiN_x with $x < 1.33$.

A typical TEM micrograph of the surface of the films deposited at smaller separation distances and/or lower ambient pressures is shown in Fig. 5a. Several droplets with dimensions of ~ 1 µm can be observed. One of these droplets was analysed by electron diffraction (Fig. 5b). The droplet consists entirely of fine α-Si polycrystallites [26] (Fig. 5b) with dimensions of 50–100 nm. The same result was obtained when performing the SAED analysis on any of the droplets.

One notices the absence of any texture within the polycrystalline zone. This means that the droplets were incident on an amorphous bed covering the single-crystal substrate. The epitaxial regrowth of the film is therefore prohibited. Another point concerns the abundance of these polycrystalline zones (droplets). There are more polycrystalline zones on the films deposited at 14 or 21 mm. Finally, we note the coexistence on the surface of some of the grown thin films of various phases – i.e. the amorphous silicon nitride, the amorphous SiN_x, the amorphous silicon and the crystalline α-Si. These zones lie at µm distances from one another. This feature is characteristic to the films obtained at smaller and intermediate pressures of NH_3.

3.4. Spectroscopic ellipsometry investigations

The homogeneous character of the films deposited by LRA, was proven by testing them optically with the ellipsometer. We observed homogeneous areas which could easily be linked to the ellipsometer light source. The samples surface and interface are planar and fairly sharp.

The SE studies have confirmed that the films obtained at larger pressure of the ambient NH_3, mainly consist of silicon nitride. A typical SE spectrum recorded for a film which was obtained at an ambient pressure of $p_0 = 1$ mbar, is given in Fig. 6 (curve a). A computation based upon the ellipsometric parameters of the refractive index, for an investigating wavelength of $\lambda = 547$ nm gives $n = 2.6$, in the case of the films obtained at $p_0 = 1$ mbar and $d = 30$ mm (curve a in Fig. 6). We note that this value is very close to $n = 2.2$ which corresponds to pure silicon nitride but is far from the value of 4.75 which is characteristic to amorphous silicon [27].

The experimental curve was then fitted with the aid of a three phases structural model. The optical properties of each phase were introduced by the Bruggeman EMA. We note that according to Ref. [28] EMA is a reliable method when applied to silicon nitride/silicon oxide/silicon multilayer structure analysis. The dielectric functions of the crystalline Si, amorphous Si, silicon nitride and silicon dioxide, were used in the fitting using the "Ellipsometry Simulation Program" [29]. The best fitting of curve a was obtained for a structure consisting of a 280 nm thick layer of Si_3N_4

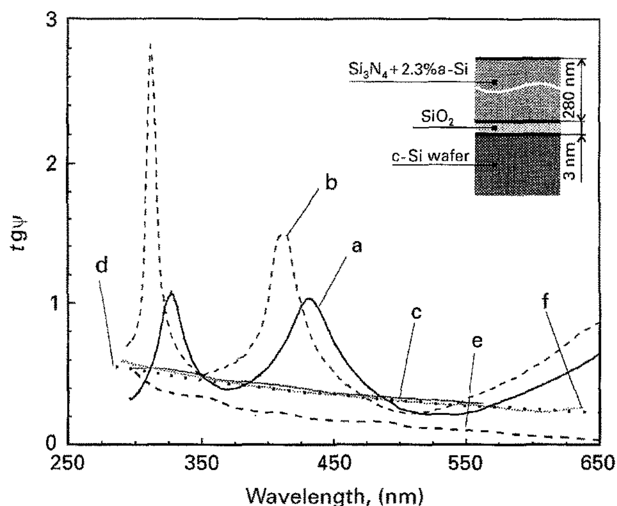

Figure 6 Spectroscopic ellipsometry spectra.
Curve (a) corresponds to a film deposited by LRA of Si in NH_3 at $p_0 = 1$ mbar and $d = 30$ mm. This curve entirely coincides with the best fitting obtained by Bruggeman EMA for a structure consisting of 280 nm Si_3N_4 with 2.3% a-Si as impurity, separated from the bulk single-crystal Si substrate by an interlayer of 3 nm SiO_2 (scheme in the right upper corner). Curve (b) is an EMA Bruggeman fitting for a structure consisting of 280 nm pure a-Si_3N_4/3 nm of SiO_2/single crystal Si substrate. Curves (c) and (d) correspond to films deposited by LRA at $p_0 = 1$ μbar, $d = 21$ mm and $d = 30$ mm, respectively. Curve (e) is recorded in case of a film deposited by laser ablation of Si in vacuum. Curve (f) is the Bruggeman EMA fitting for a structure consisting of 280 nm pure a-Si/3 nm SiO_2/single crystal Si substrate.

which includes 2.3% amorphous Si as an impurity separated from the bulk single-crystal Si substrate by an interlayer of SiO_2 of 3 nm thickness (this scheme is depicted in the right upper corner of Fig. 6). We have taken into account the native oxide layer of SiO_2 which has a similar thickness. We point out that the thickness obtained by simulation agrees with the value measured by profilometry and which was found to be in the case of this film ($p_0 = 1$ mbar, $d = 30$ mm) of ~0.3 μm. The best fitting completely superimposes in Fig. 6 with the experimentally recorded spectrum. Two other spectra which correspond to the two limit situations are also given in the figure. They correspond to the case when the upper layer of 280 nm thickness consists of pure silicon nitride (curve b), or of pure amorphous silicon (curve f). The main conclusion following from inspection of curves a, b and f in Fig. 6 is that the film obtained at $p_0 = 1$ mbar exhibits optical properties very similar to silicon nitride and quite different from those of silicon in either the amorphous or crystalline state [30].

In Fig. 6 (curve e) we have introduced the SE spectrum corresponding to the thin film deposited by laser ablation of silicon in a vacuum. This spectrum is analogous to that of the amorphous silicon (compare the curves e and f). Amorphous silicon is also dominant in the case of films obtained at a lower pressure of the ambient gas. Thus the fraction of amorphous Si is larger at a pressure of several tens of μbar, and becomes prevalent at few μbar. As a consequence, the measured SE spectrum practically reproduces the spectrum of amorphous Si (compare curves c, d and f in Fig. 6).

3.5. Electron spectroscopy studies

The top layer with a thickness of 5–6 nm, of the films was studied by both XPS and AES techniques. According to Ref. [31] the Si 2p level at 99.7 eV is shifted to 101.9 eV in Si_3N_4 and to 103.4 eV (+/− 0.2 eV) in SiO_2. On the other hand, the Si 2p line width increases with the electronegativity of the species bound to Si, from 1.2 eV in pure Si to 1.7 eV in Si_3N_4 and 2 eV for SiO_2. The Si 2p level spectra are formed by the overlapping of the lines coming from unbonded Si atoms and Si atoms chemically bonded in either Si_3N_4 or SiO_2.

The analysis of the XPS spectra recorded in case of films synthesized and deposited in NH_3, showed, in all cases, the presence of the Si–N bond (Fig. 7). The peak assigned to the Si–N bond is clearly visible for the samples deposited at higher pressures of the ambient NH_3 (i.e. for $p_0 = 0.1$ mbar and especially for $p_0 = 1$ mbar) and is much smaller for samples deposited at a pressure of ambient NH_3 of a few, up to a few tens of μbar. It is also apparent from Fig. 7, that an important contamination with oxygen is occurring. Using the peak synthesis method [31] an analysis of the spectrum reproduced in Fig. 8, gives a relative abundance for the three chemical states of Si as: 32% unbonded Si, 19% Si–N and 49% Si–O. In relative terms, then the contamination is more important in the case of films obtained at lower pressures of ambient NH_3.

Another important piece of experimental evidence was revealed by scanning the surface of the films with the aid of the facilities for "Small area XPS". It was thus observed, that the films deposited at larger pressure of 0.1–1 mbar of NH_3, exhibit a rather homogeneous composition. This is proven by the quite identical spectra recorded at different locations on the film surfaces characterized by a constant ratio between the amplitude and the total area of the peaks assigned to the different chemical bonds. On the other hand, films deposited at the smaller pressures of 1 μbar and 10 μbar, appeared to be inhomogenous.

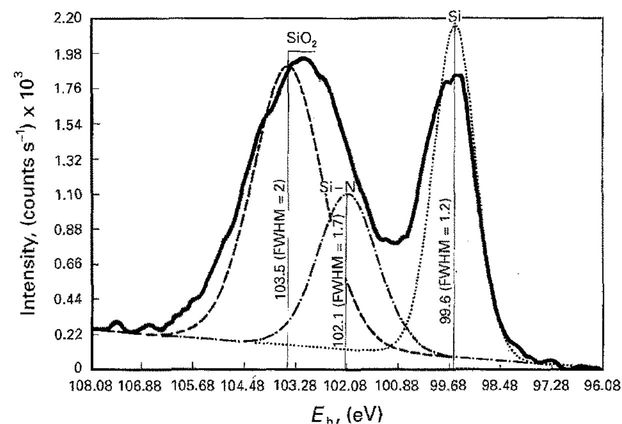

Figure 7 XPS spectrum recorded in case of a film deposited at $p_0 = 1$ mbar and $d = 30$ mm.

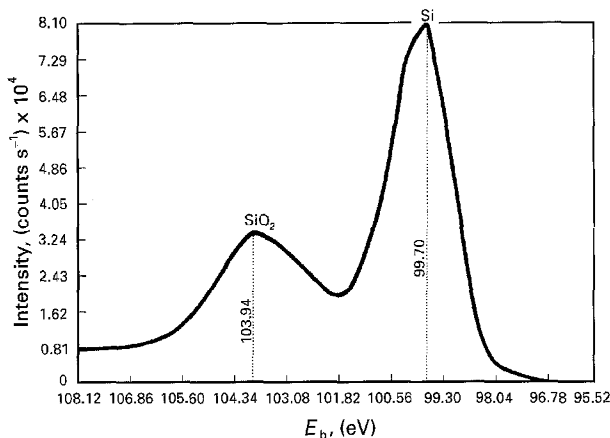

Figure 8 XPS corresponding to a zone of the surface of a film obtained at $p_0 = 10$ μbar and $d = 21$ mm.

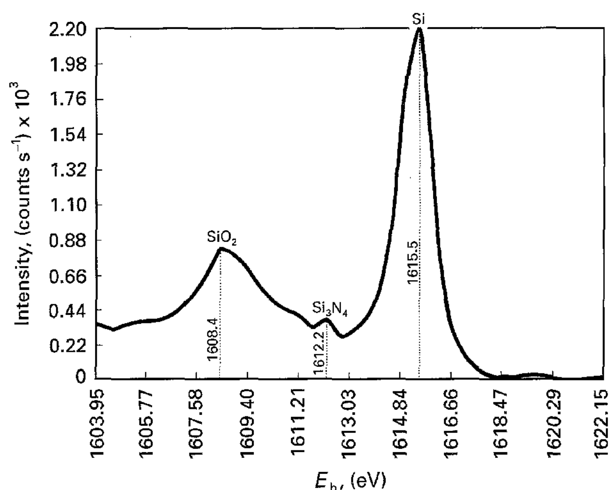

Figure 9 AES spectrum recorded in the case of a film deposited at $p_0 = 0.1$ mbar and $d = 30$ mm.

For example a location where the presence of Si_3N_4 is confirmed by the distinct peak at 102.1 eV (as in Fig. 7) is separated by only a few μm from other locations were the Si–N peak is absent and only the peak of unbonded Si and the Si–O peak could be observed (Fig. 8).

The same characteristic features were observed in the Auger spectra. The Auger Si KLL transition is found within the energy range of 1600–1650 eV [32]. According to [32], the transition Si KLL, peaks at 1616.2 eV (the corresponding Auger parameter is $\alpha = 1715.9$) in the case of unbonded Si. For the Si–N bond in Si_3N_4 this transition is shifted to 1612.2 eV ($\alpha = 1714.1$) while for the Si–O bond in SiO_2 the transition peaks at 1608.8 eV ($\alpha = 1712.2$).

As is visible in Fig. 9, both peaks are present in the recorded Auger spectra proving the coexistence of the two phases, Si_3N_4 and SiO_2. The same general trend was observed when comparing the Auger spectra of thin films prepared at different values of the NH_3 pressure, p_0. The peak pointing to the existence of the Si_3N_4 diminishes in both amplitude and area when p_0 is decreased from 1 mbar to 1 μbar.

4. Discussion

We have shown that the LRA of Si in NH_3 successfully results in the synthesis and the deposition of layers containing a prevalent quantity of silicon nitride. Silicon nitride is present as an amorphous phase. We have observed that silicon nitride is the majority phase compared with the other phases, at the highest pressures of (0.1–1) mbar of ambient NH_3 used in our experiments. Amorphous silicon is another important phase. It is prevalent at lower pressures of NH_3 (a few μbar to several tens of μbar). A third amorphous compound was identified, which is most probably amorphous nonstoichiometric silicon nitride (SiN_x, $x < 1.33$). Another important observation concerns the reduced contamination with oxygen of the layers obtained by LRA of Si in NH_3. The oxygen is present in the form of silicon dioxide only at the very top of the deposited layers.

Droplets of μm size were observed on the surface of the deposited layers. Their abundance and dimensions are larger at smaller separation distances. As for the droplets origin, we note that according to current analysis [11–15], they can be formed by two basic processes. The droplets could be sprayed from a liquid layer covering the interaction area by the recoil pressure of the ablated material [33]. Alternatively, the droplets can form by the clustering of the ablated material during the transition through the ambient gas and at impact on the collecting surface [34].

We note that our experimental observations, mostly confirm the first process. Indeed, the clustering should be more important as the ablated substance becomes cooler – i.e. the formation of more clusters (droplets) is expected after a longer transit. But, as we pointed out in Sections 3.2 and 3.3 there are significantly more droplets on films deposited at a target-collector separation distance of $d = 14$ mm than at $d = 21$ mm or at $d = 30$ mm. We consider therefore, that the droplets are expelled from a liquid phase on the target. During movement through the ambient gas they are gradually eliminated due to gravity, since the movement takes place in our experiments along a horizontal line.

The droplet geometry and especially, their composition also provide key information about the main physical phenomena involved in the LRA of Si in NH_3. Indeed, as proved by electron diffraction (Fig. 5 b), the droplets consist entirely of Si. We consequently infer that the melted material from which ablation is promoted, is in fact unreacted Si. These droplets can only be insignificantly nitridated [15] during the movement through the ambient gas and at the impact on the collector due to minimal exposure to NH_3, before solidification.

In contrast with what we have suggested in previous work [14, 15], further considerations induces us to think that there is a very small probability that the Si becomes nitridated during the existence of a liquid phase within the irradiation zone. The exposure of the liquid area in contact with the gas is at the most 1 layer of NH_3 molecules. This means that, during the existence of the liquid phase, the nitridation process cannot advance by more than a few tenths of a nm.

Of course, it is possible that gas in zones close to the irradiation area, is captured into the liquid pool by the convective fluxes found in molten substances [35]. The velocity of convection depends on the particular convection mechanism operating. For the case of thermocapillary convection, the time for one vortex turn, is $\tau \sim 100\ \mu s$. Vortices can also develop due to the recoil pressure on the liquid created by the ablated material and the plasma [35]. The corresponding initiation time of 1 vortex is $\sim 1\ \mu s$. Both these times are much longer than the total duration of the melted phase, ≥ 100 ns and thus they cannot play a significant role in feeding the gas into the liquid pool.

These restrictions impede the progress of the nitridation process during the existence of the liquid layer. As a result, during this time the nitride synthesis advances only insignificantly in the liquid phase. Consequently, the plasma recoil pressure acts upon a liquid pool of Si, and droplets entirely consisting of Si, are expelled.

The conclusions of these analyses are fully consistent with the results of a special experiment. Using the facilities for small area XPS we have positioned the investigating electron beam both inside the crater forming as an effect of the laser treatment and also away, from its border on the target surface. The results we obtained in the case of a Si target which was subjected to the action of 10^4 laser pulses, in NH_3 at $p_0 = 1$ mbar, are given in Fig. 10. We observed that the peak corresponding to the Si–N bond at 101.6 eV, is present both in the spectrum (curve a in Fig. 10) corresponding to the zone inside the crater, and also in the spectrum (curve b in Fig. 10) corresponding to a zone placed 3 mm from the crater edge. The peak completely vanishes (curve c in Fig. 10) after a short superficial cleaning (sputtering) of the investigated zone inside the crater. Even so, the target was melted to a depth hundreds of times deeper [15, 38].

The relative weight of the Si–N and Si–O bonds, inside and outside the crater were inferred by the peak

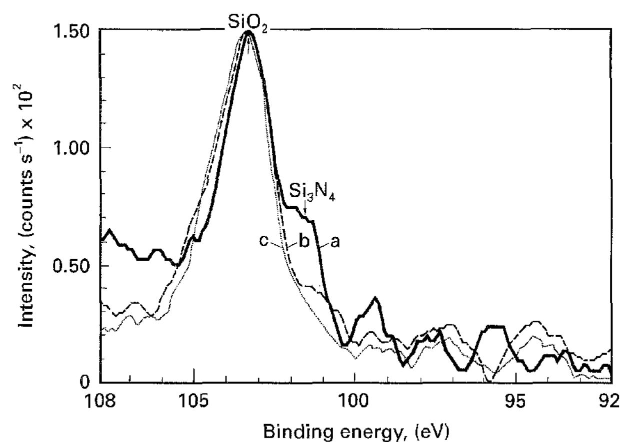

Figure 10 XPS spectra corresponding to a Si target submitted to the action of 10^4 laser pulses ($f = 10$ Hz) in ambient NH_3 at $p_0 = 1$ mbar. The curves (a) and (b) correspond respectively to the zone inside and outside (3 mm apart) the crater forming on the target surface as an effect of the multipulse laser treatment. Curve (c) corresponds to a zone inside the crater after a few minutes sputtering with a 10 keV ion beam.

TABLE I The relative abundance of the silicon nitride and silicon dioxide inside the crater and 3 mm away from its edge on the target surface

	Crater zone	A zone placed at 3 mm from crater edge
Si_3N_4	25 %	8 %
SiO_2	75 %	92 %

synthesis method [32] applied to curves a and b of Fig. 10. The results are given in Table I. From this we deduce:

(i) there is a significant presence of Si–N bonds outside the crater;

(ii) the Si–N bond, is three times more abundant inside the crater than outside it.

We observe that these results are in good agreement with the date of [39] where a careful comparison was performed of the surface processes involved in the nitridation of Si by NH_3 and in SiN_x film deposition. According to [39] at a Si substrate temperature of 860 K the nitridation process is started but remains limited. A nearly spatially uniform N chemisorption, capping all the Si surface dangling bonds in a randomly distributed way, is accomplished. A localization of the nitrogen atoms is mainly limited to the top layer in this stage.

On the other hand, inside the crater the temperature evolves to much higher values and the Si melting point is surpassed. As a result [39], higher dynamical exposure values are reached, and a stoichiometric Si_3N_4 develops at 800 °C. Nitrogen incorporation is saturated, as all the Si coordination sites are occupied by nitrogen.

We further examine the phenomena occurring after the substance leaves the laser action zone on the target surface. A hot vapour flow with a high degree of ionization is continuously leaving the irradiation area. In other words, the plasma is generated directly from the solid phase, a process which is strongly determined by the surface temperature. The plasma density and degree of ionization depend only on the absorbed laser energy. The Si plasma, rapidly recombines [40, 41] (in less than 30 ns), becomes cooler and its density strongly diminishes during its expansion in the ambient gas. Consequently, the Si plasma cannot ignite a breakdown plasma into ambient NH_3, because it simply does not mix with the gas [42, 43] (as happens with the plasma generated under the action of high-intensity TEA–CO_2 laser radiation). The Si plasma pressure exceeds significantly the pressure of the ambient gas. The gas is chased out from the areas neighbouring the laser treated zone. The gas is therefore less exposed to the focused laser beam, and is therefore only minimally involved in the plasma. This description of the phenomena occurring in zones close to the laser irradiation area, is fully supported by the absence of lines belonging to the gas species in all the time integrated OES experiments.

There are two other stages which can contribute to nitridation: the further transit through the ambient

gas in the heart of the growth chamber of the ablated substance and its impact on to the collector. We observed that both stages are strongly influenced by the pressure of the ambient gas, p_0. Indeed, the mean free path of molecules strongly diminishes with the pressure p_0 according to a p_0^{-1} law [44]. With increasing p_0, more collisions take place between the ablated substance and the gas molecules and the reaction probability increases. Also, the capacity for the NH_3 molecules to react with deposited material on the collector surface, in the time interval elapsing between the arrival of two pulses of ablated substance, increases 10^3 times when the pressure is varied from 1 μbar to 1 mbar. One therefore obtains, better progress in the nitridation reaction with increasing p_0. The process seems to be complete at $p_0 = 1$mbar, while at lower pressures there is a lack of NH_3 molecules, to react with all the Si atoms.

Gas pressure variation causes yet another, more subtle effect, related to the thermal stability [45] at different pressures of the Si_3N_4 molecule (Table II). According to the data in Table II, Si_3N_4 is stable at 2250 K at atmospheric pressure, but becomes unstable at 1600 K at a pressure of several hundreds of μbar and at 1500 K, in a vaccum. Si is a vapour at temperatures in excess of 3520 K [46], and a liquid at temperatures larger than 1690 K [30]. Si atoms can only react in the solid phase with NH_3 to form a Si_3N_4 molecule, when the gas pressure is of the order of tens or hundreds of μbar. At such pressures the Si_3N_4 molecule forms and instantaneously dissociates into either a vapour or liquid phase. The situation is better at $p_0 = 1$mbar where a small temperature window allows for the Si_3N_4 formation into a liquid phase. In conclusion we consider the reaction on to the collector surface as the most probable one. The collector surface receives enough NH_3 molecules in the time interval elapsing between the arrival of two subsequent flows of ablated substance. Also, the hot Si atoms are in contact with the NH_3 molecules for a long time before their complete cooling on the collector surface.

We also suggest a positive role for the plasma radiation on advancing the nitridation reaction during this stage. The plasma generates radiation under an extended range of wavelengths [47, 48]. This radiation can act efficiently on the NH_3 molecules adsorbed on to the collector surface and enhance the direct photolysis of the NH_3 molecules, resulting in the advent of an NH_2^+ radical. This hypothesis is still being checked.

An important argument in favour of the prevalent contribution to nitridation of the reactions taking place on the collector surface, is the experimental evidence obtained at lower NH_3 pressures. As pointed out in Sections 3.3 and 3.5, in the most sensitive range of small and intermediate pressures of NH_3 (of several μbar to several tens of μbar), the coexistence is observed in the films, of different phases. These phases include amorphous silicon nitride, amorphous silicon and amorphous nonstoichiometric products (of the type SiN_x). Which specific compound is formed, depends in our opinion, on the status of the location on which the ablation flow is incident upon. If there are enough absorbed NH_3 molecules, the process ends with the formation of stoichiometric Si_3N_4. If the amount of the NH_3 molecules is insufficient, the result is either a nonstoichiometric phase or an unreacted Si deposit.

TABLE II The thermal stability of the Si_3N_4 molecule at various pressures of the ambient gas[a]

Dissociation pressure of Si_3N_4 (equilibrium), (bar)	Temperature (K)
0.27	1606
5.5	1802
10^3	2250

[a]See Reference [45].

5. Conclusions

We have successfully extended the applications of LRA to the synthesis and deposition in a one step process of thin films with a prevalent content of silicon nitride. The films are mostly amorphous.

The best results in respect with the purity and the overall quality of the films were obtained at a pressure of 1 mbar of the ambient NH_3. The films deposited at lower pressures of NH_3 (on the order of a few μbar to a few hundreds of μbar), are in fact a mosaic of different phases such as: amorphous silicon nitride, amorphous nonstoichiometric silicon nitride and amorphous silicon.

The film quality is sometimes hampered by the presence of droplets which were expelled from a liquid phase in the laser action zone on the target. We observed that the number and dimensions of these droplets diminishes with an increase of either the separation distance between the target and collector or alternatively the pressure of ambient NH_3.

We observed that contamination with oxides stands as an essential drawback for the laser preparation of thin films of compounds not containing oxygen. By an appropriate choice of the experimental conditions (an initial vacuum lower than 10^{-6} mbar, a purity of 99.99% of NH_3, the heating of the chamber walls during the transfer operations), we succeeded in limiting the oxygen contamination to the very top layer of the deposited films.

The deposition rate of the silicon nitride thin films reached 0.3 nm per pulse at a target-collector separation distance of 14 mm. This decreased by almost one order of magnitude at a separation distance of 30 mm. The films are quite uniform and have good optical properties since they could be characterized by spectroscopic ellipsometry.

Based on the information concerning the composition and the structure of the droplets, we have demonstrated that the nitridation process does not start in the case of LRA of Si in NH_3 within the irradiation zone of the target submitted to the ablation. All experimental evidence, fully agrees with the hypothesis that silicon nitride is mostly formed on the collector, under impact of the ablated substance cloud.

Acknowledgments

The authors are thankful to M. Di Giulio for profilometry recordings and to A. Andrei for the electron spectroscopy studies.

References

1. V. I. BELYI, L. L. VASILYEVA, A. S. GINOVKER, V. A. GRITSENKO, S. M. REPISKY, S. P. SINITSA, T. P. SMIRNOVA and F. L. EDELMAN, in "Silicon Nitride in Electronics", ed. A. V. Rzhanov, (Elsevier, Amsterdam, 1988) p. 243
2. J. T. MCKINTRY, H. HU and A. H. CORIM, *J. Electrochem. Soc.*, **141** (1994) 2483.
3. J. I. STEINFELD, "Laser Induced Chemical Processes", (Plenum Press, New-York- London, (1981))
4. P. BERGONZO and I. W. BOYD, *Appl. Phys. Lett.* **63** (1993) 1757.
5. Y. NUMASAWA, K. YAMAZAKI and K. HAMANO, *Jpn. J. Appl. Phys.* **22** (1983) L792.
6. I. W. BOYD, "Laser Processing of Thin Films and Microstructures" ed. Aram Mooradian. Springer Series, 184 (1987).
7. I. URSU, R. ALEXANDRESCU, I. MORJAN and I. N. MIHAILESCU, *Infrared Phys.* **303** (1990) 271.
8. D. H. LOWNDES, D. B. GEOHEGAN, D. ERES, S. J. PENNYLOCK, D. N. MASHBURN and G. E. JELLISON, *Appl. Surf. Sci.* **36** (1989) 59.
9. Y. NUMASAWA, K. YAMAZAKI and K. HAMANO, *Jpn. J. Appl. Phys.* **22** (1983) L792.
10. B. ALLAIN and J. PERRIN, *Appl. Surf. Sci.* **36** (1989) 205.
11. I. N. MIHĂILESCU, V. CRĂCIUN, L. C. NISTOR, V. S. TEODORESCU, E. D'ANNA, G. LEGGIERI, A. LUCHES, M. MARTINO, A. PERRONE, A. V. DRIGO, S. GANATSIOS and J. ZEMEK, *J. Appl. Phys.* **70** (1991) 2123.
12. E. D'ANNA, G. LEGGIERI, A. LUCHES, M. MARTINO, P. MENGUCCI, I. N. MIHAILESCU and J. ZEMEK, "Progress in Surface Science", vol. 35 (Pergamon Press, USA 1991) p. 129.
13. E. FOGARASSY, A. SLAOUY, C. FUCHS and J. P. STOQUERT, *Appl. Surf. Sci.* **46** (1990) 195.
14. I. N. MIHĂILESCU, N. CHITICA, V. S. TEODORESCU, M. L. DE GIORGI, G. LEGGIERI, A. LUCHES, M. MARTINO, A. PERRONE, B. DUBREUIL, *J. Vac. Sci. Technol. A* **11** (1993) 2577.
15. I. N. MIHĂILESCU, N. CHITICA, L. C. NISTOR, M. POPESCU, V. S. TEODORESCU, I. URSU, A. ANDREI, A. BARBORICĂ, A. LUCHES, M. LUISA DE GIORGI, A. PERRONE, B. DUBREUIL, J. HERMANN, *J. Appl. Phys.* **74** (1993) 5781.
16. V. CRACIUN, D. CRACIUN and I. W. BOYD, *Mater. Sci. Eng. B* **18** (1993) 178.
17. F. VEGA, C. N. AFONSO, C. ORTEGA, and J. SIEJKA, *J. Appl. Phys.* **74** (1993) 963.
18. J. SOLIS, F. VEGA, C. N. AFONSO, E. GIORGIOU, D. CHARALAMBIDIS and C. FOTAKIS, *ibid.* **74** (1993) 4271.
19. A. LUCHES, G. LEGGIERI, M. MARTINO, A. PERRONE, G. MAJNI, P. MENGUCCI and I. N. MIHAILESCU, *Appl. Surf. Sci.* **79/80** (1994) 244.
20. M. L. DEGIORGI, G. LEGGIERI, A. LUCHES, M. MARTINO, A. PERRONE, G. MAJNI, P. MENGUCCI, J. ZEMEK and I. N. MIHAILESCU, *Appl. Phys. A* **60** (1995) 275.
21. E. C. PALOURA, S. LOGOTHETIDIS, S. BOULTADAKIS and S. VES, *Appl. Phys. Lett.* **59** (1991) 280.
22. J. PETALAS, S. LOGOTHETIDIS, A. MARKVITZ, E. C. PALOURA, R. L. JOHNSON and D. FUCHS, *Physica B* **185** (1993) 342.
23. D. A. G. BRUGGEMAN, *Ann. Phys. (Leipzig)* **24** (1935) 636.
24. D. E. ASPNES, *Thin Solid Films* **89** (1982) 249.
25. YI-MING XIONG, P. G. SNYDER, J. A. WOOLLAM and E. R. KROSCHE, *J. Vac. Sci. Technol. A* **10** (1992) 950.
26. ASTM 5–565.
27. E. D. PALIK, "Handbook of Optical Constants of Solids" (Academic, New York, 1985)
28. YI-MING XIONG, P. G. SNYDER, J. A. WOOLMAN, G. A. AL-JUMAILY, F. J. GAGLIARDI and L. J. MIZERKA, *Surface and Interface Analysis* **18** (1992) 124.
29. A. R. HEYD "Ellipsometry Simulation Programme" version 4.01 (MRS, University Park, PA, 1988).
30. S. W. SUN, P. J. TOBIN, J. WAHMEIR, E. REED, *J. Electrochem. Soc.: Solid State Science and Technology* **7** (1987) 1799.
31. F. ROCHET, S. RIGO, M. FROMENT, C. D'ANTERROCHES, C. MAILLOT, H. ROULET, G. DUFOUR, *Adv. Phys.* **35** (1986) 237.
32. WILLEY "Practical Surface Analysis by Auger and X-ray Photoelectron Spectroscopy", eds D. Briggs and M. P. Seah (Wiley, Chichester, 1983)
33. E. D'ANNA, G. LEGGIERI, A. LUCHES, M. MARTINO, A. V. DRIGO, I. N. MIHĂILESCU, S. GANATSIOS, *J. Appl. Phys.* **69** (1991) 1687.
34. J. C. MILLER (ed.) "Laser Ablation, Principles and Applications" (Springer-Verlag, Berlin, 1994).
35. R. V. ARUTYUNAN, V. U. BARANOV, P. A. BOLBSOV, D. D. MALYUTA and A. U. KEBRANT, "Action of Lasers Irradiation on Materials" (Nauka, Moscow, 1989) chaps. 2,3 (in Russian).
36. V. N. GOLUBEV, I. A. DOROFEEV, M. N. LIBENSON and V. I. LUCHIN, *Pis'ma v J.T.F.* **17** (1991) 1253.
37. I. N. MIKAILESAI, N. CHITICA, V. S. TEODORESCU, M. POPESCU, M. DEGIORGIO, A. LUCHES, A. PERRONE, CH. BOULMER–LEBORGNE, J. HERMANN, D. DUBREUIL, S. UDREA, A. BARBORICA and J. IOVA, *J. App. Phys.* **75** (1994).
38. I. N. MIKAILESAI, A. LITA, V. S. TEODORESCU, R. A. ESCU, E. GYORGY, A. LUCHES, M. MARTINO, A. BARBORICA, *J. Vac. Sci. Tech.* accepted.
39. L. KUBLER, J. L. BISCHOFF and D. BOLMONT, *Phys. Rev. B* **38** (1988) 13113.
40. J. HERMANN, C. BOULMER-LEBORGNE, B. DUBREUIL and I. N. MIHAILESCU, *J. Appl. Phys.* **74** (1993) 3071.
41. J. HERMANN, A. L. THOMANN, C. BOULMER-LEBORGNE, B. DUBREUIL, M. L. DEGIORGIO, A. PERRONE, A. LUCAS and I. N. MIHAILESCU, submitted to J. Appl. Phys. (July 1994)
42. I. APOSTOL, M. DINESCU, AL. HENING, I. N. MIHAILESCU, A. M. PROKHOROV, V. I. KONOV, I. URSU and N. I. CHAPLIEV, *J. Appl. Phys.* **58** (1985) 1765.
43. M. STOICA, I. N. MIHAILESCU, AL. HENING, I. URSU, A. M. PROKHOROV, P. I. NIKITIN, V. I. KONOV and A. S. SILENOK, *ibid.* **66** (1989) 5204.
44. E. W. MCDANIEL, "Collision Phenomena in Ionized Gases", vol. 2, ed. S. C. Browne (John Wiley, New York, 1964) 42.
45. Gmelins Handbook of Inorganic Chemistry, 8th ed., edited by R. J. Meyer and E. H. Erich Pietsch (Verlag Chemie, Weinheim, 1951), vol. **15B**, 602 (in German)
46. Entsiclopedia Neorganiceski Materialov, vol. **1** ed. I. M. Fedorceuko-Glorinia, Kiev (Redoktue Ukrainskoi Soretskoi enticklopedii, 1977), p. 642.
47. F. O'NEILL, I. C. E. TURCU, D. XENAKIS and M. H. R. HUTCHINSON, *Appl. Phys. Lett.* **55** (1989) 2603.
48. I. C. E. TURCU, I. N. ROSS and G. J. TALLENTS, *ibid.* (1993) 3046.

Received 15 June 1995
and accepted 20 November 1995